BBA - Bioenergetics 1860 (2019) 375–382

Contents lists available at ScienceDirect

BBA - Bioenergetics

journal homepage: www.elsevier.com/locate/bbabio

Insights into the ubiquinol/dioxygen binding and proton relay pathways of the alternative oxidase

Tomoo Shiba[a,*,1], Daniel Ken Inaoka[b,c,d,*,1], Gen Takahashi[a], Chiaki Tsuge[d], Yasutoshi Kido[b,e], Luke Young[f], Satoshi Ueda[a], Emmanuel Oluwadare Balogun[a,d,g], Takeshi Nara[h], Teruki Honma[i], Akiko Tanaka[i], Masayuki Inoue[j], Hiroyuki Saimoto[k], Shigeharu Harada[a], Anthony L. Moore[f], Kiyoshi Kita[b,d,c]

[a] Department of Applied Biology, Graduate School of Science and Technology, Kyoto Institute of Technology, Sakyo-ku, Matsugasaki, Kyoto 606-8585, Japan
[b] School of Tropical Medicine and Global Health, Nagasaki University, Sakamoto 1-12-4, Nagasaki 852-8523, Japan
[c] Department of Host-Defense Biochemistry, Institute of Tropical Medicine (NEKKEN), Nagasaki University, Sakamoto 1-12-4, Nagasaki 852-8523, Japan
[d] Department of Biomedical Chemistry, Graduate School of Medicine, The University of Tokyo, Bunkyo-ku, Hongo 7-3-1, Tokyo 113-0033, Japan
[e] Department of Parasitology, Graduate School of Medicine, Osaka City University, Abeno-ku, Asahimachi 1-4-3, Osaka 545-8585, Japan
[f] Biochemistry and Biomedicine, School of Life Sciences, University of Sussex, Falmer, Brighton, BN1 9QG, UK
[g] Department of Biochemistry, Ahmadu Bello University, Zaria 2222, Nigeria
[h] Department of Molecular and Cellular Parasitology, Juntendo University School of Medicine, Bunkyo-ku, Hongo 2-1-1, Tokyo, 113-8421, Japan
[i] Systems and Structural Biology Center, RIKEN, Tsurumi, Suehiro 1-7-22, Yokohama, Kanagawa 230-0045, Japan
[j] Graduate School of Pharmaceutical Sciences, The University of Tokyo, Bunkyo-ku, Hongo 7-3-1, Tokyo 113-0033, Japan
[k] Department of Chemistry and Biotechnology, Graduate School of Engineering, Tottori University, Koyamacho-Minami 4, Tottori 680-8552, Japan

ARTICLE INFO

Keywords:
Alternative oxidase
Ubiquinol/dioxygen binding
Proton relay pathway
Trypanosoma brucei
Ferulenol
Competitive inhibitor

ABSTRACT

The alternative oxidase (AOX) is a monotopic diiron carboxylate protein which catalyzes the four-electron reduction of dioxygen to water by ubiquinol. Although we have recently determined the crystal structure of *Trypanosoma brucei* AOX (TAO) in the presence and absence of ascofuranone (AF) derivatives (which are potent mixed type inhibitors) the mechanism by which ubiquinol and dioxygen binds to TAO remain inconclusive. In this article, ferulenol was identified as the first competitive inhibitor of AOX which has been used to probe the binding of ubiquinol. Surface plasmon resonance reveals that AF is a *quasi*-irreversible inhibitor of TAO whilst ferulenol binding is completely reversible. The structure of the TAO-ferulenol complex, determined at 2.7 Å, provided insights into ubiquinol binding and has also identified a potential dioxygen molecule bound in a *side-on* conformation to the diiron center for the first time.

1. Introduction

The alternative oxidases (AOX) are cyanide-insensitive quinol oxidases found ubiquitously in plants and also in many protists and fungi [1]. AOX is a single polypeptide which oxidizes two quinol molecules and catalyzes the transfer of four electrons to a molecule of dioxygen producing two molecules of water non-protonmotively [1]. AOX has many functions including thermogenesis, stress tolerance and maintenance of mitochondrial and cellular homeostasis [1]. Whilst physiological information of AOX has increased through the advancement of genome sequencing and gene manipulation, a biochemical understanding of the mechanism of AOX action is limited due of the difficulties in purifying large quantities of AOX in its active form.

The mitochondrion of *Trypanosoma brucei*, a protozoan parasite causing African sleeping sickness in humans and nagana in cattle, utilises AOX dependent respiration in the blood stream of mammalian host to generate cytosolic ATP [2]. We have previously used a bacterial system to overexpress the Trypanosomal alternative oxidase (TAO) in an *Escherichia coli* strain deficient in heme biosynthesis [3]. Using this system, the expression of TAO was high enough to purify the protein in large quantities, resulting in the first membrane-bound diiron enzyme to be crystallized [4,5].

Biochemical studies on the mechanism of dioxygen reduction by AOX have been limited because the protein lacks chromophores or any other spectroscopic method of analysis. Some potential diiron redox cycle intermediates of AOXs, however have been detected by FTIR [6]

* Corresponding authors.
E-mail addresses: tshiba@kit.ac.jp (T. Shiba), danielken@nagasaki-u.ac.jp (D.K. Inaoka).
[1] These authors contributed equally to this work.

https://doi.org/10.1016/j.bbabio.2019.03.008
Received 20 December 2018; Accepted 20 March 2019
Available online 22 March 2019
0005-2728/

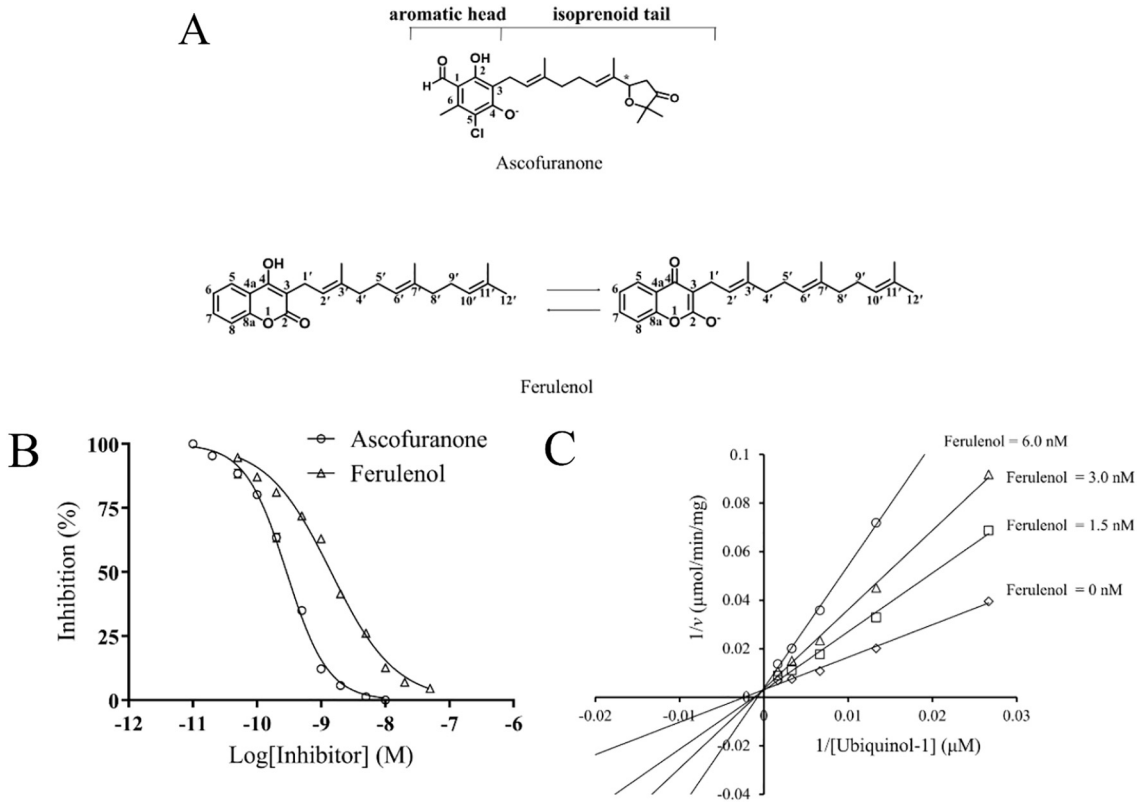

Fig. 1. Structure of ferulenol and ascofuranone. (A) The chemical structure of ferulenol (Top) and ascofuranone (bottom). (B) Inhibition curve of quinol oxidase activity of TAO by ferulenol and ascofuranone. The calculated IC_{50} for ferulenol and ascofuranone was 1.42 ± 0.102 nM and 0.288 ± 0.012 nM, respectively. (**C**) Double reciprocal plot of [quinol] vs [V] under increasing concentrations of ferulenol. The inhibition of ferulenol was determined as competitive because of intersection of each graph at Y-axis. The K_i of ferulenol was calculated as 1.33 ± 0.157 nM.

and EPR [7,8]. However, all of those studies performed so far have focussed on the nature of diiron center, with scarce information on either the binding of ubiquinol and dioxygen or the mechanism underlying the electron transfer events.

A competitive inhibitor of substrate binding is an important tool to study the reaction mechanism of an enzyme [9]. Furthermore, competitive inhibitors can be used to trap and analyze reaction intermediates [9–11].

We have previously reported that ascofuranone (AF) (Fig. 1A), an antibiotic isolated from *Acremonium sclerotigenum* [12] is the most potent inhibitor of AOX family of enzymes identified to date [2,3]. In mammals, AF was originally identified in anticancer [13] and antiviral [14] screenings, however, the target of AF was unknown until recently. We have identified AF and its derivatives as potent inhibitors of dihydroorotate dehydrogenase (HsDHODH), the rate-limiting step in the pyrimidine de novo biosynthesis pathway [15]. Structure activity relationship of AF identified the functional groups necessary for TAO [16] as well as HsDHODH [15] inhibition. Although, AF is a structural analogue of ubiquinol, it is a mixed-type rather than a competitive inhibitor [4], with respect to TAO. In order to identify a competitive inhibitor of AOX, we screened over 50 quinone/quinol binding site inhibitors against TAO and discovered that ferulenol is a novel potent AOX inhibitor (Fig. 1A). Ferulenol is a sesquiterpene prenylated coumarin derivative, a natural product originally isolated from *Ferula communis* [17]. Ferulenol has previously been reported to be a potent inhibitor of *Plasmodium falciparum* malate:quinone oxidoreductase (MQO, IC_{50} = 0.057 μM) [18], a weak inhibitor of the rat mitochondrial respiratory enzyme succinate ubiquinone reductase (SQR, IC_{50} = 17 μM) [19] and an inhibitor of rat and bacterial vitamin K epoxide reductase (VKOR) with IC_{50}s of 0.098 and 0.200 μM [20], respectively. MQO is a mitochondrial inner membrane bound enzyme catalyzing the oxidation of malate and reduction of ubiquinone producing oxaloacetate and ubiquinol [18]. MQO is functionally equivalent to mammalian malate dehydrogenase, a member of the TCA cycle, however, they have no homology each other [18]. SQR is a mitochondrial membrane protein catalyzing the electron transfer from succinate to respiratory quinones, a key reaction connecting tricarboxylic acid cycle to the respiratory chain. VKOR is an endoplasmic reticulum (ER) membrane protein catalyzing quinone-dependent protein disulfide bond formation essential for γ-glutamyl carboxylation reactions necessary for blood coagulation, maintenance of ER and cellular redox balance in animals [21], unicellular eukaryotes [22] and bacteria [20], respectively.

In this study, we investigated the mechanism of TAO inhibition by ferulenol and discovered it to be a potent competitive inhibitor of TAO activity with respect to the binding of ubiquinol. We demonstrate, by surface plasmon resonance, that the dissociation of AF is extremely slow making it a *quasi*-irreversible inhibitor whilst ferulenol, in comparison, dissociates relatively fast. We obtained a crystal structure of the TAO-ferulenol complex, at 2.7 Å, which has provided the first structural insight into the mechanism of ubiquinol/ubiquinone recognition by AOX. Importantly it has revealed that, in the presence of ferulenol, a molecule of dioxygen is bound *side-on* to the diiron center and potential proton relay pathways leading to generation of water and ubiquinol are identified. Such findings have provided us with not only important data on the initial oxidation steps following the binding of ubiquinol but also on how dioxygen is reduced by the AOX family of enzymes.

2. Material and methods

2.1. In vitro assay

5.0×10^4 of bloodstream form parasites were incubated in HMI-9 medium with different concentrations (333 μM − 2.6 pM) of ferulenol or AF in 96-well plates for 18 h at 37 °C and 5% CO_2, in a total volume of 100 μl. Each compound was diluted in DMSO and each concentration was prepared in triplicate. After incubation, 10 μl Alamar Blue stock solution (TREK Diagnostic Systems) was added to each well and incubated for more 6 h. Absorbance at 570 nm and 600 nm was measured and growth rate of trypanosomes was calculated by using the following equation.

$$C_{red}(\varepsilon_{red})\lambda_1 + C_{ox}(\varepsilon_{ox})\,\lambda_1 = A\lambda_1$$
$$C_{red}(\varepsilon_{red})\lambda_2 + C_{ox}(\varepsilon_{ox})\,\lambda_2 = A\lambda_2$$

Minimum inhibitory concentration (MIC) was determined as the concentration to kill 100% of parasites by microscopic observation. The same procedure was performed also in the presence of 5 mM glycerol.

To calculate the percent difference in reduction between treated and control cells, the following equation was used according to manufacturer instruction:

$$\frac{(\varepsilon_{ox})\lambda_2\,(A\lambda_1 - A'\lambda_1) - (\varepsilon_{ox})\lambda_1(A\lambda_2 - A'\lambda_2)}{(\varepsilon_{ox})\lambda_2\,(A^o\lambda_1 - A'\lambda_1) - (\varepsilon_{ox})\lambda_1(A^o\lambda_2 - A'\lambda_2)} \times 100$$

where, C_{red} and C_{ox} corresponds to the concentration of reduced and oxidized form Alamar Blue, respectively and ε_{ox} is the molar extinction coefficient of its oxidized form. A, A' and A° is the absorbance of test, positive control and negative control wells, respectively. Finally, λ_1 is 570 nm, λ_2 is 600 nm and ε_{ox} of oxidized form of Alamar Blue at λ_1 and λ_2 is 80,586 and 117,216, respectively.

2.2. Inhibition kinetics

TAO was purified essentially as described previously [5]. IC_{50} of AF and ferulenol was determined by measuring the relative ubiquinol oxidase activity of rTAO in the presence of varying concentrations of inhibitors. Ubiquinol oxidase activity was measured by recording the increase in the absorbance due to ubiquinone-1 formation at 278 nm (Shimadzu spectrophotometer, UV-3000). Reactions were started by the addition of 150 μM ubiquinol-1 ($\varepsilon_{278} = 15\,mM^{-1}\,cm^{-1}$) after 2 min pre-incubation at 25 °C, in the presence of 150 ng membrane fraction of *E. coli* expressing rTAO, varying concentrations of inhibitors and 50 mM Tris–HCl (pH 7.4) without detergents. Each plot from the IC_{50} graph, represent the average of three independent experiments and analyzed by GraphPad Prism 7.01.

The mechanism of TAO inhibition by ferulenol was measured by recording the quinol oxidase activity at varying concentrations of ubiquinol-1 (final concentrations 37.5 to 600 μM) and ferulenol (0, 1.5, 3.0, 6.0 nM) in the presence of 75 ng of purified rTAO in 50 mM Tris–HCl (pH 7.4) containing 0.05% (w/v) octaethylene glycol-monodecylether (C10E8) using 1 ml black-quartz cuvette [4]. The obtained raw data were analyzed by GraphPad Prism 7.01.

2.3. Surface plasmon resonance

The binding kinetics of AF and ferulenol to TAO was analyzed by SPR using BiacoreT200 instrument (GE Healthcare Japan) at 25 °C. Purified rTAO was covalently immobilized to two (one for each inhibitor) Series S sensor chips CM5 using amine coupling kits (GE Healthcare Japan) according to manufacturer's protocol. Briefly, carboxyl groups in the immobilization matrix were first activated by treatment with a fresh mixture of 200 mM 1-ethyl-3-(3-dimethylaminopropyl) carbodiimide hydrochloride and 50 mM N-hydroxysuccinimide (NHS) at 10 μl/min for 7 min. TAO diluted to 9.8 μg/ml in 10 mM sodium acetate pH 5.5 was then injected over the surface at 10 μl/min for 7 min where the immobilization level of 21,000 resonance units (RU) was reached. Finally, unreacted NHS esters were blocked by 1 M ethanolamine hydrochloride pH 8.5 at 10 μl/min for 7 min. The effect of AF and ferulenol in binding the TAO was analyzed by single cycle kinetics. TAO inhibitors diluted to 31.25, 62.50, 125, 250 and 500 nM wash buffer containing 10 mM HEPES pH 7.4, 150 mM NaCl, 0.05% (w/w) Tween 20 and 5% (v/v) DMSO were automatically injected in serial mode over the sensor chip at rate of 30 μl/min for 60 s. After injection of 500 nM inhibitor, the sensor chip was rinsed with wash buffer for 600 s to monitor the dissociation. The binding responses of the two inhibitors were measure in RU in real time at 10 Hz. Raw sensorgram data were reference subtracted and blank subtracted before kinetic and affinity analysis. Dissociation constant (K_D) was calculated using Biacore T200 Evaluation software by fitting the recorded data to a 1:1 interaction model. In the case of AF, the sensor chip surface could not be regenerated because of its *quasi*-irreversible binding nature to TAO.

2.4. Preparation of TAO-ferulenol complex crystals

The alternative oxidase from *T. b. brucei* was crystallized according to the method described previously [5] using 28–34% (w/v) PEG 400, 100 mM imidazole buffer pH 7.4 and 500 mM potassium formate as the reservoir solution. The crystals of the TAO-ferulenol complex were prepared by soaking TAO crystals in the cryo-protectant solution [50% (w/v) PEG 400, 500 mM potassium formate and 100 mM imidazole buffer pH 7.4] supplemented with 1 mM ferulenol for 60 min at 20 °C. The crystals ware mounted in a nylon loop and flash-frozen in a stream of gaseous nitrogen at 100 K.

2.5. Data collection and structural refinement

The diffraction data of TAO-ferulenol complex crystal was collected to 2.7 Å resolution at 100 K at SPring-8 beamline BL41XU (Harima, Japan). The data set was processed and scaled with HKL2000 [23]. The crystal belongs to the orthorhombic space group *C*2 with unit cell parameters; $a = 228.0$, $b = 138.0$, $c = 63.1$ Å and $\beta = 105.9°$. In the crystal structure, there were four monomers in the asymmetric unit. The initial model of TAO-ferulenol complex was determined by molecular replacement (MR) using the CCB-TAO complex [PDB code: 3W54; [5]] as a search model. The program, Phaser [24] in CCP4i was used for MR. Manual re-building and crystallographic refinement of all structures were performed using the COOT [25] and REFMAC5 [26]. The structure was refined by amplitude-based twin-refinement in REFMAC5 [26] to final R_{work}/R_{free} values of 0.192/0.247. On average, about 30 residues of N- and C-termini of TAO were missing as a result of flexibility. Stereochemistry of the refined structure was validated by PROCHECK [27] and Ramachandran plots indicated that no amino acid residues were detected in energetically unfavorable regions. Data collection and structural refinement statistics are summarized in Supplemental information (Table S1). Figures showing protein structures were prepared with the graphics program PyMOL (http://www.pymol.org/). The atomic coordinates and structure factors have been deposited in the Protein Data Bank, www.pdb.org (PDB ID codes 5ZDP).

3. Results

3.1. Mechanism of ferulenol inhibition

In an attempt to identify a suitable competitive inhibitor of TAO ubiquinol oxidase activity, over 50 known inhibitors of quinol or quinone utilizing enzymes were screened. All classical inhibitors of respiratory chain such as rotenone (complex I) [28], atpenin A5 (complex II) [29], antimycin A (complex III) [30] and brequinar (dihydroorotate dehydrogenase) [31] were ineffective against TAO. However, screening resulted in the discovery of ferulenol (Fig. 1A), a known inhibitor of MQO [18], SQR [19] and VKOR [20], as a potent inhibitor of TAO with

Table 1
Inhibition kinetic parameters of ferulenol and ascofuranone at enzymatic and cellular level. All parameters, if not stated, are shown in nM.

	IC_{50} (rTAO)	K_i	k_{on} ($M^{-1}\,s^{-1}$)	k_{off} (s^{-1})	K_D	Inhibition	IC_{50} (BSF)	
							− glycerol	+ 5 mM glycerol
Ascofuranone	0.288	n.a.	2.167×10^6	1.045×10^{-4}	0.048	Mixed	0.66	0.05
Ferulenol	1.42	1.33	1.372×10^6	0.0914	66.62	Competitive	3300	1100

an IC_{50} of 1.42 nM (Fig. 1B, Table 1). In comparison, AF has an IC_{50} of 0.288 nM (Fig. 1B, Table 1). The mechanism of inhibition by ferulenol was determined using purified rTAO and as can be seen in Fig. 1C, ferulenol is a potent competitive inhibitor of ubiquinol oxidation with a K_i of 1.33 nM.

3.2. Binding mode of ferulenol

In order to determine the mechanism of binding of ferulenol (and thereby ubiquinol) by TAO, we solved the crystal structure of TAO in complex with ferulenol at 2.7 Å (Table S1, PDB code 5ZDP). In the crystal structure, four monomers are observed within the asymmetric unit. There are no significant structural differences amongst monomers in the asymmetric unit, as indicated by root-mean-square (r.m.s.) deviations (0.34–0.50 Å) of the superimposed Cα positions (Table S2). The overall enzyme structures of the TAO-ferulenol complex are comparable to those of ligand-free TAO and TAO-ascofuranone derivative complexes [5], as shown by similar value of r.m.s. deviations ranging from 0.28 to 0.86 Å (Table S2). The binding site of ferulenol is located near the membrane surface between helices α1 and α4 (Fig. 2A). The aromatic head moiety is recognised by extensive hydrophilic and hydrophobic interactions with Arg96, Arg118, Leu122, Glu123, Ala216, Thr219 and Tyr220 (Fig. 2B, Table S3). All of these residues are conserved amongst AOX from all other species identified to date [1]. Furthermore, the isoprenoid-tail moiety interacts with Cys95, Arg96, Leu122, Thr186, Ile189, Leu212 and Glu215 through van der Waals contacts (Fig. 2B, Table S3). The isoprenoid-tails are bending at C1′ position of the isoprenoid-tail (the angle C3-C1′-C2′ are 117–121°) filled into the hydrophobic cavity between α1 and α4 (Fig. 2A). The bending of isoprenoid-tail is mainly caused by Cys95, Arg96, Leu212 and Glu215 through hydrophobic interactions (Fig. 2C).

3.3. The diiron center of TAO-ferulenol complex structure

In the crystal structures of TAO both complexed with either AF derivatives or ferulenol, the diiron center (Fe2-OH^--Fe1) in all chains is coordinated by four glutamate residues (Glu123, Glu162, Glu213 and Glu269) which are essential for quinol oxidase activity [5,32]. In the structure of TAO complexed with colletochlorin B (CCB), two additional electron densities, corresponding to two water molecules (W2 and W1) could be identified (Supplemental Fig. S1). W1 coordinates Fe2 (W2-W1-Fe2-OH^--Fe1) in all chains with W1-Fe2 distance ranging from 2.5 Å to 2.0 Å. Importantly, in the TAO-ferulenol structure an extra elongated density was observed which is clearly larger than a single water molecule. Indeed, the electron density map could be fitted perfectly by a molecule of dioxygen bound at a *side-on* conformation to Fe2 (Supplemental Fig. S2), however, detailed analysis of higher resolution crystal structures obtained under anaerobic condition is required to fully validate this hypothesis. Interestingly, the positioning and binding of the proposed dioxygen molecule within the active-site is very similar to that observed in other non-heme iron oxygenases such as naphthalene dioxygenase [33] and carbazole 1,9a-dioxygenase [34] (see Supplemental Fig. S2), as well as non-enzyme iron complexes [35]. The position of the two histidines (His165 and His269) in TAO-ferulenol complex are within 4.5 Å around diiron center as previously observed in all TAO-ligand complexed structures.

3.4. Comparison with ascofuranone derivatives

Recently we described the structure of TAO in complex with AF derivatives AF2779OH and CCB [5]. In all of the inhibitor-complex structures, the OH2 from the benzene moiety is hydrogen bonded with Arg118 and Thr219 resulting in the chlorine group being 4.06 Å from Fe2 and the 1-formyl group within 3.49 Å of the Thr219-CH_3λ without apparently any binding to OH4. However, a comprehensive structure activity relationship (SAR) of several AF derivatives [16] revealed that OH2 is not essential whilst OH4 and 1-formyl groups are essential for TAO inhibition. Considering the low resolution of our previous TAO structures, we have subsequently concluded that the AF derivatives were modeled into the density map with their benzene moiety rotated 180° at C1' axis. In the corrected binding mode, Arg118 and Thr219 interact with the OH4 thereby resulting in the 1-formyl group being positioned close to the water molecule that coordinates Fe2 (W1, Fig. 2C), which is consistent with our previous SAR results [16]. The updated versions of crystal structures of TAO in complex with AF2779OH and colletochlorin B were deposited with new PDB IDs of 5ZDR and 5ZDQ, respectively.

The position of the isoprenoid-tail of ferulenol and AF derivatives completely overlaps between the two types of inhibitor (Fig. 2D). Hence, similar to the AF derivatives (the angle C3-C1'-C2' are 103–120°), the isoprenoid-tail of ferulenol is kinked at C1' position about 120 degree (Fig. 2D). The 4-hydroxycoumarin head of ferulenol as well as the aromatic head from AF derivatives are located at the same plane (Fig. 2D). The C3 positions of ferulenol and AF derivatives are almost same. The hydroxyl group at the C4 position within AF derivatives (in its ionized form) (see Fig. 1A), which is important for interacting with Arg118 and Thr219, is located between the ether oxygen atom at position 1 and the ketone oxygen atom at the position 2 of the ferulenol aromatic ring (Fig. 2D). Of particular interest is the finding that additional hydrogen bonding between the ketone oxygen atom at the C2 of ferulenol and Arg96 can also be observed (Fig. 2B–D).

3.5. Binding kinetics of AF and ferulenol

The binding kinetics of several drugs have been correlated to their biological activities. For example, the potent antiviral activity of duranavir, a FDA-approved HIV protease inhibitor, was linked to its slow dissociation constant (k_{off}) compared to its derivatives [36]. The binding kinetics analysis of AF in comparison to that of ferulenol was determined using surface plasmon resonance (SPR) (Fig. 3). The SPR curve of both inhibitors showed best fitting using 1:1 binding model. Fig. 3A shows that binding of AF is characterized by biphasic dissociation. The fast phase is characteristic of a fast dissociation or weakly-bound AF, and a slow phase characterized by a tightly-bound AF which dissociates from TAO extremely slowly (Fig. 3A). From the total amount of AF dissociated from TAO, the weakly and tightly bound moieties of AF represent the minority and majority fraction, respectively. The weakly bound AF fraction becomes more pronounced at higher concentrations of inhibitor as shown by SPR analysis in Fig. 3A. The association constant (k_{on}) of AF and ferulenol (Fig. 3B) are of a similar magnitude (2.167×10^6 and 1.372×10^6, respectively) whilst the dissociation constant (k_{off}) of AF ($k_{off} = 1.045 \times 10^{-4}$) was 875 times lower than that of ferulenol ($k_{off} = 0.0914$) (Table 1). In practice, AF is considered to be a *quasi*-irreversible inhibitor with a binding

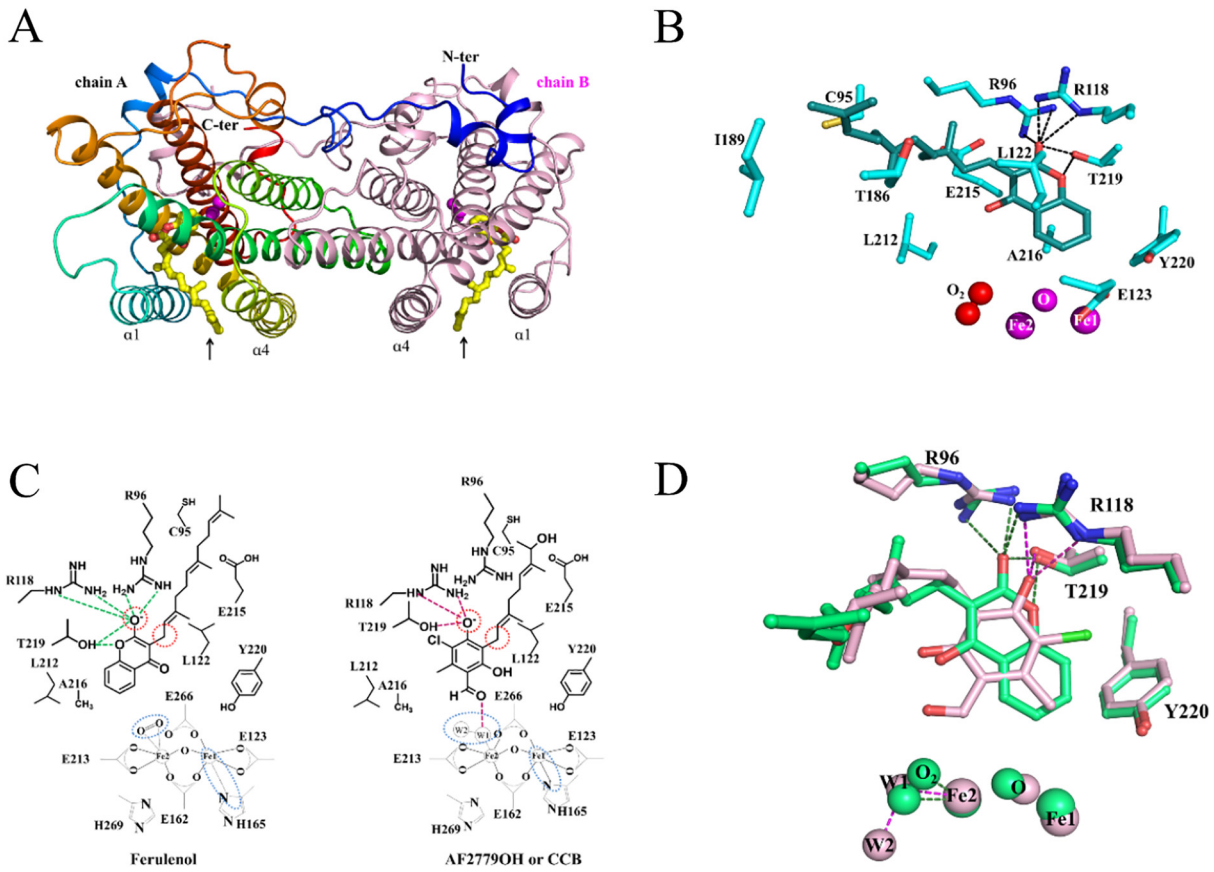

Fig. 2. Binding mode of TAO and ferulenol. (A) Overall structure of TAO-ferulenol complex showing its binding site (arrows) located between α1 and α4 helices. (B) Representative binding mode of ferulenol in TAO. The residues which interact with ferulenol (dark cyan) are shown as sticks, respectively. N, O and S atoms are coloured in blue, red and yellow, respectively. Magenta spheres represent the diiron center (Fe-OH$^-$-Fe). Dioxygen molecule is shown as red spheres. Hydrogen bonds between TAO and ferulenol are shown as dotted lines. (C) Schematic comparison of the binding mode of ferulenol and AF derivatives. The interactions of residues within the binding site and ferulenol are shown as green dotted lines (left panel) whereas those which interact with AF derivatives are shown as magenta dotted lines (right panel). The common and different feature between them is highlighted as dotted red and blue circles, respectively. (D) Superimposed between TAO-ferulenol (green) and TAO-AF2779OH (light pink) complex. The residues which interact with ferulenol and AF2779OH are shown as green and light pink sticks, respectively. Tyr220, an important residue for the enzymatic activity is also shown as green (TAO-ferulenol) and light pink (TAO-AF2779OH) sticks, respectively. Hydrogen bonds between TAO and its inhibitors are shown as dotted lines (ferulenol; green, AF2779OH; magenta).

affinity constant (K_D) of 0.048 nM (Fig. 3A, Table 1). Ferulenol, however, shows a classical characteristic of a reversible inhibitor namely a K_D of 66.6 nM (Fig. 3B, Table 1). It is possible to distinguish between tight and slow-binding inhibitors by determining if there is a time dependent increase in the $IC_{50,}$ a characteristic of a slow-binding inhibitor [37]. No change in the IC_{50} was detected for both AF and ferulenol even when the incubation time was increased from 2 to 10 min (data not shown) suggesting that both AF and ferulenol are indeed tight-binding inhibitors of TAO.

3.6. Trypanocidal activity of ferulenol

AF inhibits purified TAO with an IC_{50} of 0.288 nM and the growth of the bloodstream form of the parasite at similar magnitudes (IC_{50} of

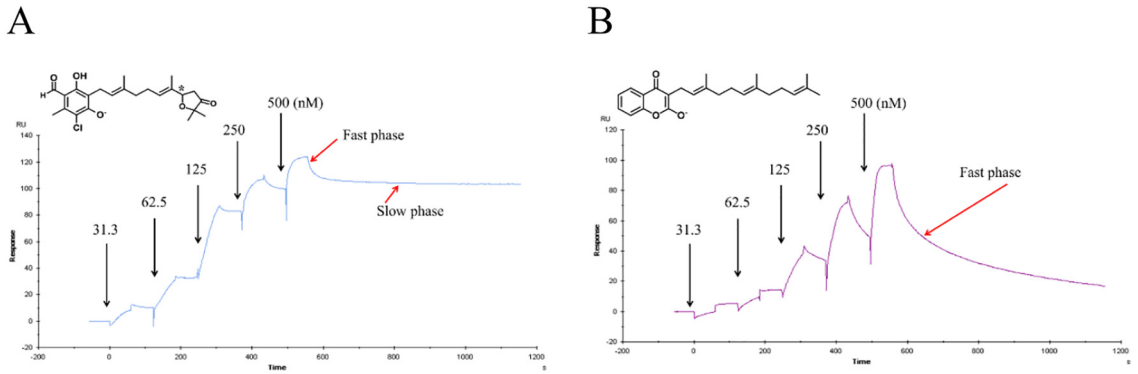

Fig. 3. Surface plasmon resonance binding analysis of TAO inhibitors. Sensorgram of ascofuranone (A) and Ferulenol (B). The numbers on the graph and the black arrows indicate the concentrations and the time points where the inhibitor was injected into the sensor chip, respectively. The weakly bound ascofuranone and ferulenol which dissociate fast (fast phase) and the tightly bound ascofuranone which dissociates extremely slow (slow phase) are indicated in red arrow.

0.66 nM). Growth inhibition by AF is synergistically potentiated by the presence of 5 mM glycerol (IC_{50} decreases to 0.05 nM) due to its inhibition of glycerol kinase (Table 1) [38,39]. Glycerol kinase is an important enzyme for ATP production via substrate level phosphorylation in the blood stream form of *T. b. brucei* through its reverse reaction [11]. Since ferulenol inhibits TAO with an IC_{50} of 1.42 nM (Fig. 1B, Table 1), a similar order of trypanocidal activity was anticipated. However, under the same assay condition as for AF, ferulenol was effective only at concentrations of 3.3 μM (without glycerol) and 1.1 μM (with glycerol, Table 1). Therefore, even though ferulenol is a potent inhibitor of TAO and does bind at the same site as AF, we suggest that the difference in in vitro efficacy discussed above can be explained by the binding kinetics summarized in Table 1.

4. Discussion

4.1. Mechanism of ubiquinol binding and reduction by TAO

The complete reduction of dioxygen to water requires four electrons and four protons and several mechanisms have been suggested to account for the net oxidation of two ubiquinols [40,41]. So far, only one binding site for mixed-type and competitive inhibitors (versus ubiquinol) has been identified in all of the TAO-ligand structures crystallized to date (Fig. 3). Such data strongly indicates that the two ubiquinol molecules bind consecutively and not concomitantly in the same pocket. As illustrated by the complex structures highlighted in Figs. 2 and 3, Arg96, Arg118 and Thr219 are key residues which interact both with ferulenol and the AF derivatives and mutation of any of these residues results in approximately 90% inhibition of TAO catalytic activity [42].

In an attempt to determine the nature of ubiquinol binding within AOX, we have used the SPR analysis (Fig. 3) and the complex structures of TAO-ferulenol and TAO-AF derivatives (Fig. 2D) to model ubiquinol within the binding pocket (Fig. 4).

We propose that the initial event is characterized by a weak binding of ubiquinol to Arg96 (Fig. 4A) in a manner similar to that observed with ferulenol from the SPR analysis (Fig. 3B). Once bound to Arg96, the benzene ring of ubiquinol is re-positioned such that its OH1 group becomes tightly bound to Arg118/Thr219 (Fig. 4B) similar to that observed with AF derivatives (Fig. 2C and D). Such a tightly bound mode of ubiquinol positions the OH4 group to a distance of 4.0 Å, 4.7 Å and 3.7 Å (Fig. 4B) to the bridging oxo group, Fe2 and the water coordinating Fe2 (W1), respectively. Such a realignment facilitates electron transfer from ubiquinol OH4 to the diiron center (Fig. 4B).

We suggest that upon the binding of the first ubiquinol, one proton and one electron from OH4 is transferred directly to the oxo group by proton-coupled electron transfer (PCET, Fig. 4). The second electron is transferred directly to a previously reported stable tyrosyl radical in the fully oxidized state (Tyr220) forming a tyrosinate residue [6].

Given the orientation of quinol within the pocket, it is likely that the proton from ubiquinol OH1 is transferred to solvent through Arg118/Asp100 or Thr219/Arg96/Glu215 pathway (Fig. 4). Both potential proton relay pathways are connected to outside solvent (Fig. 4). In order to maintain the reaction stoichiometry, protons must be transferred into the diiron core, which can be achieved from the solvent via a water (W3) and His269 pathway (Fig. 4B).

Following oxidation of ubiquinol, there is a shift in the interaction of ketone O1 from Arg118 to Arg96. At this point, ubiquinone will only interact weakly with the enzyme thereby facilitating its release (Fig. 4A). Importantly all residues involved in the binding of ubiquinol/ubiquinone (Arg96, Arg118 and Thr219) are conserved amongst the AOX family, supporting our notion of the critical role they play in catalysis. Following the first ubiquinol oxidation step, both irons still remain oxidized and thus do not react with dioxygen, consistent with our previous suggestions that the diiron core remains dioxygen inactive even after such a two electron reduction step [6].

The reaction of the second quinol with the protein is harder to predict, as the conformational changes predicted in our previously published electrochemical work [6] suggest there is a protonation and change in the environment of at least one carboxylate following the first reduction step. Even so, it is unlikely that a single carboxylate will reveal the presence of a second active site, and therefore we feel it is safe to assume that the second equivalent of quinol must bind within the same cavity. As such, the reaction is predicted to proceed in a similar manner to that described for the first quinol, with two electrons reducing the diiron core, one proton being used to form molecular water and one proton being donated to solvent through the proton relay pathway. This fully reduced structure has been predicted to be the dioxygen reactive species, with the mechanistic predictions being discussed in a previous paper [6].

Such a mechanism of ubiquinol/ubiquinone binding and oxidation is supported by the differences in the dissociation pattern between

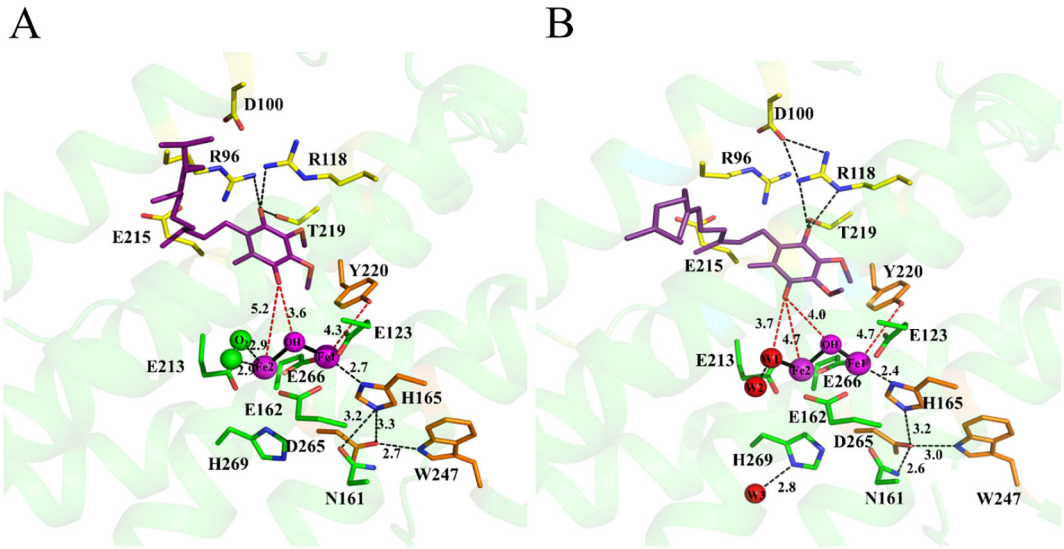

Fig. 4. Proposed interaction of bound ubiquinol with the first and second ligation sphere around diiron center. TAO-ubiquinol complex model based on the TAO-ferulenol (A) and TAO-CCB complex structures (B). The hydrogen bonds are shown in black dotted lines. The red dotted lines are important for the enzymatic reaction of TAO.

ascofuranone and ferulenol revealed by SPR analysis, the competitive inhibitory nature of ferulenol and finally structures of TAO-in the presence of inhibitors. Our model also accounts for the biphasic and monophasic dissociation nature of ascofuranone and ferulenol, respectively. From the SPR analysis, two binding modes of AF could be observed, namely a weakly and a tightly bound species whereas only the weakly binding species could be detected for ferulenol. Interestingly, a dual binding mode of ubiquinone species within the active site has also been reported for *E. coli* succinate:ubiquinone oxido:reductase (SQR), in which the co-crystallization with different types of ubiquinone analogs resulted in different binding modes [43]. The analogy between SQR and AOX is very interesting because under physiological conditions they utilize the same substrates as AOX, however, they catalyze the opposite redox reaction. Thus, there is a possibility that even though SQR and AOX are completely distinct enzymes, they probably share a conserved mechanism of substrate binding and catalysis. Such a kind of conservation of non-related enzymes has also been reported for the fumarate reduction site of family 1A dihydroorotate dehydrogenase and quinol:fumarate reductases [10,44].

4.2. Ascofuranone and ferulenol as transition state analogues of TAO

As far as drug development is concerned, the principal benefits of a *quasi*-irreversible inhibitor are the achievement of prolonged efficacy under low doses and reduced drug resistance. This is demonstrated by many clinically used drugs such as aspirin, celecoxib, vigatatrin, procarbazine, lanzoprazole, celegiline, orlistat and sulbactan which inhibit their respective target in irreversible manner [45]. In that sense, the *quasi*-irreversible nature of AF demonstrated by SPR analysis emphasize not only the superiority of ascofuranone as a drug candidate to combat African trypanosomiasis, but also the necessity to design ferulenol derivatives with much lower dissociation constants in order to achieve satisfactory trypanocidal activity.

Interestingly, several tight binding inhibitors have been shown to be transition state (TS) analogs such as Immucillin H and its derivatives. Such compounds have been shown to be potent inhibitors of purine nucleotide phosphorylase, 5′methylthioadenosine phosphorylase and 5′-Methylthioadenosine/adenosylhomocysteine nucleosidase [46]. TS analogs have also been described as compounds that bind to the enzyme catalytic site inducing conformational changes that normally occur with the enzyme's reactants [47]. In other words, a TS analog mimics the TS geometry of the enzyme during the catalytic cycle. Currently, there are approximately a dozen FDA approved HIV protease inhibitors that are widely considered as TS analogs [47]. Oseltamivir (Tamiflu) a potent influenza neuraminidase inhibitor, has also been reported to bind to the target in a conformation matching that of the TS [48]. The tight binding property of a TS analog is well documented [49–51] and is characterized by a K_m/K_D ratio higher than 10^5 orders of magnitude [50,52,53]. Considering that TAO has a minimum K_m of 338 μM for its substrate, ubiquinol [4], the K_m/K_D ratio of AF has been calculated to be 7×10^6 whilst that for ferulenol is 5×10^3. Although, more evidences from kinetic isotope effects and computational chemistry are necessary to further understand the TS from an enzyme, our current analysis suggests that AF and ferulenol possess the potential to be good TS and substrate/product analogues of TAO, respectively.

5. Conclusion

In this study, we report on the first experimental discovery of a potent and competitive inhibitor of TAO and also provide some valuable structural information on the mechanism of ubiquinol oxidation by the alternative oxidases. Of particular importance was the finding that binding of ferulenol to TAO appears to trap a potential dioxygen molecule bound *side-on* to the Fe2 in the complex structure. Although *side-on* binding of dioxygen to iron-proteins [33,34], as well as non-protein iron complexes [35,54], have previously been reported, to our knowledge this is the first report of a dioxygen bound *side-on* to a diiron protein. Due to the limited resolution of TAO-ferulenol complex structure, such observation requires further studies using different approaches in order to validate the dioxygen binding site in TAO.

Transparency document

The Transparency document associated with this article can be found, in online version.

Acknowledgement

We thank all staff members of beamline BL44XU at SPring-8 for their help with X-ray diffraction data collection.

Funding source

This work was supported in part by Infectious Disease Control from the Science and Technology Research Partnership for Sustainable Development (SATREPS, nos. 10000284 to K.K. and 14425718 to D.K.I.); a Grant-in-aid for the Bilateral Joint Research Project (no. 16035611-000722 to K.K.) and Grant-in-aid for Scientific Research on Priority Areas 18073004 (to K.K.) and Creative Scientific Research Grant 18GS0314 (to K.K.) from the Japan Society for the Promotion of Science; a Grant-in-aid from the Program for the Promotion of Basic and Applied Research for Innovations in Bio-Oriented Industry (BRAIN) (no. 26020A to S.H. and K.K.); a Grant-in-aid for Scientific Research (B) 16K19114 to D.K.I and (C) 23570131 and 26234567 to T.S. and The Leading Initiative for Excellent Young Researchers (LEADER) 16811362 to D.K.I. from the Japanese Ministry of Education, Science, Culture, Sports and Technology (MEXT). This work was also supported by the Japanese Initiative for Progress of Research on Infectious Diseases for Global Epidemic (JP18fm0208027 to D.K.I. and JP18fm0208020 to Y.K.) from Agency for Medical Research and Development (AMED). Grant-in-aid for research on emerging and re-emerging infectious diseases from the Japanese Ministry of Health and Welfare (to K.K.). A.L.M. gratefully acknowledges BBSRC for financial support and with K.K. the Prime Ministers Initiative 2 (Connect – British Council) fund for collaborative twinning.

Declaration of interests

The authors declare no competing interest exist.

Appendix A. Supplementary data

Supplementary data to this article can be found online at https://doi.org/10.1016/j.bbabio.2019.03.008.

References

[1] A.L. Moore, T. Shiba, L. Young, S. Harada, K. Kita, K. Ito, Unraveling the heater: new insights into the structure of the alternative oxidase, Annu. Rev. Plant Biol. 64 (2013) 637–663.
[2] N. Minagawa, Y. Yabu, K. Kita, K. Nagai, N. Ohta, K. Meguro, S. Sakajo, A. Yoshimoto, An antibiotic, ascofuranone, specifically inhibits respiration and *in vitro* growth of long slender bloodstream forms of *Trypanosoma brucei brucei*, Mol. Biochem. Parasitol. 84 (1997) 271–280.
[3] Y. Fukai, H. Amino, H. Hirawake, Y. Yabu, N. Ohta, N. Minagawa, S. Sakajo, A. Yoshimoto, K. Nagai, S. Takamiya, S. Kojima, K. Kita, Functional expression of the ascofuranone-sensitive *Trypanosoma brucei brucei* alternative oxidase in the cytoplasmic membrane of *Escherichia coli*, Comp. Biochem. Physiol. C Pharmacol. Toxicol. Endocrinol. 124 (1999) 141–148.
[4] Y. Kido, K. Sakamoto, K. Nakamura, M. Harada, T. Suzuki, Y. Yabu, H. Saimoto, F. Yamakura, D. Ohmori, A. Moore, S. Harada, K. Kita, Purification and kinetic characterization of recombinant alternative oxidase from *Trypanosoma brucei brucei*, Biochim. Biophys. Acta 1797 (2010) 443–450.
[5] T. Shiba, Y. Kido, K. Sakamoto, D.K. Inaoka, C. Tsuge, R. Tatsumi, G. Takahashi, E.O. Balogun, T. Nara, T. Aoki, T. Honma, A. Tanaka, M. Inoue, S. Matsuoka,

H. Saimoto, A.L. Moore, S. Harada, K. Kita, Structure of the trypanosome cyanide-insensitive alternative oxidase, Proc. Natl. Acad. Sci. U. S. A. 110 (2013) 4580–4585.
[6] A. Marechal, Y. Kido, K. Kita, A.L. Moore, P.R. Rich, Three redox states of *Trypanosoma brucei* alternative oxidase identified by infrared spectroscopy and electrochemistry, J. Biol. Chem. 284 (2009) 31827–31833.
[7] A.L. Moore, J.E. Carre, C. Affourtit, M.S. Albury, P.G. Crichton, K. Kita, P. Heathcote, Compelling EPR evidence that the alternative oxidase is a diiron carboxylate protein, Biochim. Biophys. Acta 1777 (2008) 327–330.
[8] D.A. Berthold, N. Voevodskaya, P. Stenmark, A. Graslund, P. Nordlund, EPR studies of the mitochondrial alternative oxidase. Evidence for a diiron carboxylate center, J. Biol. Chem. 277 (2002) 43608–43614.
[9] J.M. Aucoin, E.J. Pishko, D.P. Baker, E.R. Kantrowitz, Engineered complementation in *Escherichia coli* aspartate transcarbamoylase - Heterotropic regulation by quaternary structure stabilization, J. Biol. Chem. 271 (1996) 29865–29869.
[10] D.K. Inaoka, K. Sakamoto, H. Shimizu, T. Shiba, G. Kurisu, T. Nara, T. Aoki, K. Kita, S. Harada, Structures of *Trypanosoma cruzi* dihydroorotate dehydrogenase complexed with substrates and products: atomic resolution insights into mechanisms of dihydroorotate oxidation and fumarate reduction, Biochemistry 47 (2008) 10881–10891.
[11] E.O. Balogun, D.K. Inaoka, T. Shiba, Y. Kido, C. Tsuge, T. Nara, T. Aoki, T. Honma, A. Tanaka, M. Inoue, S. Matsuoka, P.A. Michels, K. Kita, S. Harada, Molecular basis for the reverse reaction of African human trypanosomes glycerol kinase, Mol. Microbiol. 94 (2014) 1315–1329.
[12] Y. Hijikawa, M. Matsuzaki, S. Suzuki, D.K. Inaoka, R. Tatsumi, Y. Kido, K. Kita, Re-identification of the ascofuranone-producing fungus *Ascochyta viciae* as *Acremonium sclerotigenum*, J. Antibiot. 70 (2017) 304–307.
[13] J. Magae, S. Suzuki, K. Nagai, M. Yamasaki, K. Ando, G. Tamura, In vitro effects of an antitumor antibiotic, ascofuranone, on the murine immune system, Cancer Res. 46 (1986) 1073–1078.
[14] G. Tamura, S. Suzuki, A. Takatsuki, K. Ando, K. Arima, Ascochlorin, a new antibiotic, found by the paper-disc agar-diffusion method. I. Isolation, biological and chemical properties of ascochlorin. (studies on antiviral and antitumor antibiotics. I), J. Antibiot. 21 (1968) 539–544.
[15] Y. Miyazaki, D.K. Inaoka, T. Shiba, H. Saimoto, T. Sakura, E. Amalia, Y. Kido, C. Sakai, M. Nakamura, A.L. Moore, S. Harada, K. Kita, Selective cytotoxicity of dihydroorotate dehydrogenase inhibitors to human cancer cells under hypoxia and nutrient-deprived conditions, Front. Pharmacol. 9 (2018).
[16] H. Saimoto, Y. Kido, Y. Haga, K. Sakamoto, K. Kita, Pharmacophore identification of ascofuranone, potent inhibitor of cyanide-insensitive alternative oxidase of *Trypanosoma brucei*, J. Biochem. 153 (2013) 267–273.
[17] P. Teresa Jde, M.A. Villaseco, J.M. Hernandez, J.R. Moran, J.G. Urones, M. Grande, Complex acetylenes from the roots of *Ferula communis*, Planta Med. (1986) 458–462.
[18] E.D. Hartuti, D.K. Inaoka, K. Komatsuya, Y. Miyazaki, R.J. Miller, W. Xinying, M. Sadikin, E.E. Prabandari, D. Waluyo, M. Kuroda, E. Amalia, Y. Matsuo, N.B. Nugroho, H. Saimoto, A. Pramisandi, Y.I. Watanabe, M. Mori, K. Shiomi, E.O. Balogun, T. Shiba, S. Harada, T. Nozaki, K. Kita, Biochemical studies of membrane bound *Plasmodium falciparum* mitochondrial L-malate:quinone oxidoreductase, a potential drug target, Biochim. Biophys. Acta 1859 (2017) 191–200.
[19] M. Lahouel, R. Zini, A. Zellagui, S. Rhouati, P.A. Carrupt, D. Morin, Ferulenol specifically inhibits succinate ubiquinone reductase at the level of the ubiquinone cycle, Biochem. Biophys. Res. Commun. 355 (2007) 252–257.
[20] W. Li, S. Schulman, R.J. Dutton, D. Boyd, J. Beckwith, T.A. Rapoport, Structure of a bacterial homologue of vitamin K epoxide reductase, Nature 463 (2010) 507–512.
[21] T. Li, C.Y. Chang, D.Y. Jin, P.J. Lin, A. Khvorova, D.W. Stafford, Identification of the gene for vitamin K epoxide reductase, Nature 427 (2004) 541–544.
[22] L.A. Rutkevich, D.B. Williams, Vitamin K epoxide reductase contributes to protein disulfide formation and redox homeostasis within the endoplasmic reticulum, Mol. Biol. Cell 23 (2012) 2017–2027.
[23] Z. Otwinowski, W. Minor, Processing of X-ray diffraction data collected in oscillation mode, Macromol. Crystallogr. Pt A 276 (1997) 307–326.
[24] A.J. McCoy, R.W. Grosse-Kunstleve, P.D. Adams, M.D. Winn, L.C. Storoni, R.J. Read, Phaser crystallographic software, J. Appl. Crystallogr. 40 (2007) 658–674.
[25] P. Emsley, K. Cowtan, Coot: model-building tools for molecular graphics, Acta Crystallogr. D Biol. Crystallogr. 60 (2004) 2126–2132.
[26] G.N. Murshudov, A.A. Vagin, E.J. Dodson, Refinement of macromolecular structures by the maximum-likelihood method, Acta Crystallogr. D Biol. Crystallogr. 53 (1997) 240–255.
[27] R.A. Laskowski, M.W. Macarthur, D.S. Moss, J.M. Thornton, Procheck - a program to check the stereochemical quality of protein structures, J. Appl. Crystallogr. 26 (1993) 283–291.
[28] M.E. Teeter, M.L. Baginsky, Y. Hatefi, Ectopic inhibition of the complexes of the electron transport system by rotenone, piericidin A, demerol and antimycin A, Biochim. Biophys. Acta 172 (1969) 331–333.
[29] H. Miyadera, K. Shiomi, H. Ui, Y. Yamaguchi, R. Masuma, H. Tomoda, H. Miyoshi, A. Osanai, K. Kita, S. Omura, Atpenins, potent and specific inhibitors of mitochondrial complex II (succinate-ubiquinone oxidoreductase), Proc. Natl. Acad. Sci. U. S. A. 100 (2003) 473–477.
[30] Z. Zhang, L. Huang, V.M. Shulmeister, Y.I. Chi, K.K. Kim, L.W. Hung, A.R. Crofts, E.A. Berry, S.H. Kim, Electron transfer by domain movement in cytochrome bc_1, Nature 392 (1998) 677–684.
[31] S.F. Chen, R.L. Ruben, D.L. Dexter, Mechanism of action of the novel anticancer agent 6-fluoro-2-(2′-fluoro-1,1′-biphenyl-4-yl)-3-methyl-4-quinolinecarbo xylic acid sodium salt (NSC 368390): inhibition of *de novo* pyrimidine nucleotide biosynthesis, Cancer Res. 46 (1986) 5014–5019.
[32] K. Nakamura, K. Sakamoto, Y. Kido, Y. Fujimoto, T. Suzuki, M. Suzuki, Y. Yabu, N. Ohta, A. Tsuda, M. Onuma, K. Kita, Mutational analysis of the *Trypanosoma vivax* alternative oxidase: the E(X)6Y motif is conserved in both mitochondrial alternative oxidase and plastid terminal oxidase and is indispensable for enzyme activity, Biochem. Biophys. Res. Commun. 334 (2005) 593–600.
[33] A. Karlsson, J.V. Parales, R.E. Parales, D.T. Gibson, H. Eklund, S. Ramaswamy, Crystal structure of naphthalene dioxygenase: *side-on* binding of dioxygen to iron, Science 299 (2003) 1039–1042.
[34] K. Inoue, Y. Usami, Y. Ashikawa, H. Noguchi, T. Umeda, A. Yamagami-Ashikawa, T. Horisaki, H. Uchimura, T. Terada, S. Nakamura, K. Shimizu, H. Habe, H. Yamane, Z. Fujimoto, H. Nojiri, Structural basis of the divergent oxygenation reactions catalyzed by the rieske nonheme iron oxygenase carbazole 1,9a-dioxygenase, Appl. Environ. Microbiol. 80 (2014) 2821–2832.
[35] J. Cho, S. Jeon, S.A. Wilson, L.V. Liu, E.A. Kang, J.J. Braymer, M.H. Lim, B. Hedman, K.O. Hodgson, J.S. Valentine, E.I. Solomon, W. Nam, Structure and reactivity of a mononuclear non-haem iron(III)-peroxo complex, Nature 478 (2011) 502–505.
[36] I. Dierynck, M. De Wit, E. Gustin, I. Keuleers, J. Vandersmissen, S. Hallenberger, K. Hertogs, Binding kinetics of darunavir to human immunodeficiency virus type 1 protease explain the potent antiviral activity and high genetic barrier, J. Virol. 81 (2007) 13845–13851.
[37] S.G. Waley, The kinetics of slow-binding and slow, tight-binding inhibition: the effects of substrate depletion, Biochem. J., 294 (Pt 1) (1993) 195–200.
[38] E.O. Balogun, D.K. Inaoka, T. Shiba, Y. Kido, T. Nara, T. Aoki, T. Honma, A. Tanaka, M. Inoue, S. Matsuoka, P.A. Michels, S. Harada, K. Kita, Biochemical characterization of highly active *Trypanosoma brucei* gambiense glycerol kinase, a promising drug target, J. Biochem. 154 (2013) 77–84.
[39] Y. Yabu, T. Suzuki, C. Nihei, N. Minagawa, T. Hosokawa, K. Nagai, K. Kita, N. Ohta, Chemotherapeutic efficacy of ascofuranone in *Trypanosoma vivax*-infected mice without glycerol, Parasitol. Int. 55 (2006) 39–43.
[40] C. Affourtit, M.S. Albury, P.G. Crichton, A.L. Moore, Exploring the molecular nature of alternative oxidase regulation and catalysis, FEBS Lett. 510 (2002) 121–126.
[41] B.M. Luke Young, Tomoo Shiba, Shigeharu Harada, Daniel Ken Inaoka, Kiyoshi Kita and Anthony L. Moore, Structure and mechanism of action of the alternative quinol oxidases., in: K.T. Cramer W. (Ed.) Cytochrome Complexes: Evolution, Structures, Energy Transduction, and Signaling. Advances in Photosynthesis and Respiration (Including Bioenergy and Related Processes), Springer, Dordrecht, Place Published, 2016, pp. 375–394.
[42] B. May, L. Young, M. Albury, D.K. Inaoka, K. Kita, A.L. Moore, Investigation into the ubiquinol-binding site of the trypanosomal alternative oxidase, Biochim. Biophys. Acta 1857 (2016) e41 BBA) - Bioenergetics.
[43] R. Horsefield, V. Yankovskaya, G. Sexton, W. Whittingham, K. Shiomi, S. Omura, B. Byrne, G. Cecchini, S. Iwata, Structural and computational analysis of the quinone-binding site of complex II (succinate-ubiquinone oxidoreductase): a mechanism of electron transfer and proton conduction during ubiquinone reduction, J. Biol. Chem. 281 (2006) 7309–7316.
[44] H. Shimizu, A. Osanai, K. Sakamoto, D.K. Inaoka, T. Shiba, S. Harada, K. Kita, Crystal structure of mitochondrial quinol-fumarate reductase from the parasitic nematode *Ascaris suum*, J. Biochem. 151 (2012) 589–592.
[45] S. Nunez, J. Venhorst, C.G. Kruse, Target-drug interactions: first principles and their application to drug discovery, Drug Discov. Today 17 (2012) 10–22.
[46] V.L. Schramm, Enzymatic transition states, transition-state analogs, dynamics, thermodynamics, and lifetimes, Annu. Rev. Biochem. 80 (2011) 703–732.
[47] V.L. Schramm, Transition states, analogues, and drug development, ACS Chem. Biol. 8 (2013) 71–81.
[48] G. Speciale, A.J. Thompson, G.J. Davies, S.J. Williams, Dissecting conformational contributions to glycosidase catalysis and inhibition, Curr. Opin. Struct. Biol. 28 (2014) 1–13.
[49] J.A. Gutierrez, M. Luo, V. Singh, L. Li, R.L. Brown, G.E. Norris, G.B. Evans, R.H. Furneaux, P.C. Tyler, G.F. Painter, D.H. Lenz, V.L. Schramm, Picomolar inhibitors as transition-state probes of 5′-methylthioadenosine nucleosidases, ACS Chem. Biol. 2 (2007) 725–734.
[50] A.S. Murkin, P.C. Tyler, V.L. Schramm, Transition-state interactions revealed in purine nucleoside phosphorylase by binding isotope effects, J. Am. Chem. Soc. 130 (2008) 2166–2167.
[51] R. Wolfenden, Thermodynamic and extrathermodynamic requirements of enzyme catalysis, Biophys. Chem. 105 (2003) 559–572.
[52] V.L. Schramm, Enzymatic transition state theory and transition state analogue design, J. Biol. Chem. 282 (2007) 28297–28300.
[53] A. Rinaldo-Matthis, C. Wing, M. Ghanem, H. Deng, P. Wu, A. Gupta, P.C. Tyler, G.B. Evans, R.H. Furneaux, S.C. Almo, C.C. Wang, V.L. Schramm, Inhibition and structure of *Trichomonas vaginalis* purine nucleoside phosphorylase with picomolar transition state analogues, Biochemistry 46 (2007) 659–668.
[54] S. Hong, K.D. Sutherlin, J. Park, E. Kwon, M.A. Siegler, E.I. Solomon, W. Nam, Crystallographic and spectroscopic characterization and reactivities of a mononuclear non-haem iron(III)-superoxo complex, Nat. Commun. 5 (2014) 5440.